J. Fluid Mech. (2018), *vol.* 843, *pp.* 29–52. © Cambridge University Press 2018
doi:10.1017/jfm.2018.115

Sound generation by turbulent premixed flames

Ali Haghiri[1,†], Mohsen Talei[1], Michael J. Brear[1] and Evatt R. Hawkes[2,3]

[1]Department of Mechanical Engineering, University of Melbourne, VIC 3010, Australia

[2]School of Photovoltaic and Renewable Energy Engineering, University of New South Wales, Sydney 2052, Australia

[3]School of Mechanical and Manufacturing Engineering, University of New South Wales, Sydney 2052, Australia

(Received 24 December 2016; revised 2 January 2018; accepted 24 January 2018; first published online 19 March 2018)

This paper presents a numerical study of the sound generated by turbulent, premixed flames. Direct numerical simulations (DNS) of two round jet flames with equivalence ratios of 0.7 and 1.0 are first carried out. Single-step chemistry is employed to reduce the computational cost, and care is taken to resolve both the near and far fields and to avoid noise reflections at the outflow boundaries. Several significant features of these two flames are noted. These include the monopolar nature of the sound from both flames, the stoichiometric flame being significantly louder than the lean flame, the observed frequency of peak acoustic spectral amplitude being consistent with prior experimental studies and the importance of so-called 'flame annihilation' events as acoustic sources. A simple model that relates these observed annihilation events to the far-field sound is then proposed, demonstrating a surprisingly high degree of correlation with the far-field sound from the DNS. This model is consistent with earlier works that view a premixed turbulent flame as a distribution of acoustic sources, and provides a physical explanation for the well-known monopolar content of the sound radiated by premixed turbulent flames.

Key words: aeroacoustics, combustion, turbulent flows

1. Introduction

Combustion noise plays a key role in the instability of many combustion systems (Strahle 1978; Docquier & Candel 2002; Lieuwen 2012; Dowling & Mahmoudi 2015; Ihme 2017). The noise generated by turbulent premixed flames deserves special attention since they are common in contemporary, low-emission gas turbines.

In one of the earlier studies of combustion noise, Smith & Kilham (1963) experimentally investigated sound generation by open, turbulent, premixed flames. Like several later works, they observed that the radiated sound was predominantly monopolar, and they argued that the emitted sound originated from monopolar sources throughout the flame. In the same year, Bragg (1963) proposed a theory to describe the relationship between the sound production and combustion by assuming that the generated noise was the result of changes in the flame volume, which was

† Email address for correspondence: a.haghiri@student.unimelb.edu.au

https://doi.org/10.1017/jfm.2018.115 Published online by Cambridge University Press

assumed to be directly proportional to changes in the rate of heat release rate. Many subsequent theoretical studies of sound generation by turbulent premixed flames have also attempted to relate the radiated sound to changes in the flame volume or the heat release rate e.g. Hurle *et al.* (1968), Strahle (1978), Kotake & Takamoto (1990), Dowling (1992), Schuller, Durox & Candel (2003), Candel, Durox & Schuller (2004), Rajaram & Lieuwen (2009), Swaminathan *et al.* (2011*a*,*b*), Liu (2015).

There are several numerical studies on sound generation by turbulent flames using large-eddy simulation (LES) e.g. Bui *et al.* (2005), Birbaud *et al.* (2006), Flemming, Sadiki & Janicka (2007), Bui, Schröder & Meinke (2008), Bui *et al.* (2009), Ihme, Pitsch & Bodony (2009), Ihme & Pitsch (2012), Silva *et al.* (2013), Zhang *et al.* (2013), Livebardon *et al.* (2015). Although the significance of the heat release rate fluctuations was confirmed by these studies, varying levels of agreement between LES and experiment was observed (Flemming *et al.* 2007; Bui *et al.* 2009) and several sources of uncertainty such as sub-grid modelling (Ihme *et al.* 2009) and grid resolution (Ihme *et al.* 2009; Silva *et al.* 2013) were found. Nonetheless, LES appears to be the only plausible tool for examining sound generation in practical turbulent flames.

In contrast to LES, direct numerical simulation (DNS) should not suffer from problems associated with grid resolution or sub-grid modelling. However, DNS of sound generation by unconfined premixed flames is relatively rare (e.g. Miyauchi, Tanahashi & Li 2001; Zhao & Frankel 2001; Tanahashi *et al.* 2002; Talei, Brear & Hawkes 2012*a*) because of the computational cost incurred by resolving both the flame and the radiated sound simultaneously, and the sensitivity of the acoustic field to numerical issues that are particularly challenging in combusting flows (Zhao & Frankel 2001; Talei, Brear & Hawkes 2014). As a result, all previous DNS studies appear to either feature a large one- or two-dimensional domain or a relatively small three-dimensional configuration (Miyauchi *et al.* 2001; Tanahashi *et al.* 2002). Once again, a common feature of these studies were the importance of heat release rate fluctuations as a source of noise.

Flame annihilation is one mechanism that can lead to large fluctuations of the heat release rate in premixed flames (Kidin *et al.* 1988; Schuller *et al.* 2003; Candel *et al.* 2004; Talei, Brear & Hawkes 2011; Brear *et al.* 2012; Talei *et al.* 2012*a*; Talei, Hawkes & Brear 2012*b*; Talei *et al.* 2014; Jiménez *et al.* 2015). During annihilation, flame surfaces collide with each other, leading to rapid consumption of the unburned gas trapped between the flame surfaces, and can therefore produce noise. In a number of theoretical and numerical studies of laminar flame annihilation, Talei *et al.* (2011, 2012*a*,*b*, 2014) investigated the impact of key flame parameters such as flame thickness, flame speed, Zel'dovich number, temperature ratio and Lewis number on flame annihilation and the produced sound. However, the significance of annihilation events in noise generation by turbulent premixed flames appears to have received no examination, even though they have been observed in numerous non-acoustic studies of turbulent, premixed flames (e.g. Echekki, Chen & Gran 1996; Balachandran *et al.* 2005; Griffiths *et al.* 2015).

The aim of this paper is therefore twofold. First, we present three-dimensional DNS of sound generation by open turbulent premixed flames. Two turbulent, methane–air flames are studied with equivalence ratios $\phi = 0.7$ and 1.0. Second, the significance of annihilation events will be examined using a simple model that is based on one of our previous studies (Talei *et al.* 2012*a*).

https://doi.org/10.1017/jfm.2018.115 Published online by Cambridge University Press

2. Governing equations

The governing equations for the conservation of mass, momentum, total energy and reactant species mass fraction are solved using a single-step, irreversible chemical reaction. The non-dimensionalised forms of the equations of motion are obtained using the flow premixture quantities, where the superscript '*' represents dimensional values and the subscript *ref* corresponds to the values of the reactant at the inlet boundary:

$$\left.\begin{aligned} &\boldsymbol{x}_j = \frac{\boldsymbol{x}_j^*}{D}, \quad t = \frac{t^* c_{ref}}{D}, \quad \boldsymbol{u}_j = \frac{\boldsymbol{u}_j^*}{c_{ref}}, \quad \rho = \frac{\rho^*}{\rho_{ref}}, \quad T = \frac{T^*}{(\gamma-1)T_{ref}}, \\ &Y_R = \frac{Y_R^*}{Y_{R,\,ref}}, \quad p = \frac{p^*}{\rho_{ref} c_{ref}^2} \quad \text{and} \quad \mu = \frac{\mu^*}{\mu_{ref}}. \end{aligned}\right\} \tag{2.1}$$

In the above, $\boldsymbol{x}$ and t are the spatial coordinate vector and time, respectively. In addition, c is the sonic velocity, $\boldsymbol{u}_j$ is the j-component of velocity vector, ρ is the mixture density, T is the temperature, γ is the heat capacity ratio and considered to be 1.4, Y_R is the reactant mass fraction (progress variable), p is the pressure, D is the jet diameter and μ is the dynamic viscosity where its variation with temperature is modelled as $= (T/T_{ref})^{0.76}$ (Poinsot, Echekki & Mungal 1992). The following non-dimensional parameters are also defined:

$$\left.\begin{aligned} &Re = \left(\frac{c\,D}{\nu}\right)_{ref}, \quad Pr = \left(\frac{\nu}{D_{th}}\right)_{ref}, \quad Le = \left(\frac{D_{th}}{D_m}\right)_{ref} = 1, \\ &Da = \left(\frac{\Lambda\, D}{c}\right)_{ref} \quad \text{and} \quad Sc = Le\ Pr, \end{aligned}\right\} \tag{2.2}$$

where Re is the acoustic Reynolds number, Pr is the Prandtl number, Sc is the Schmidt number, Le is the Lewis number, Da is the Damköhler number, D_{th} is the thermal diffusivity coefficient, D_m is the binary mass diffusion coefficient, Λ is the pre-exponential factor in the Arrhenius law and ν is the kinematic viscosity.

Using these parameters, the non-dimensional form of the governing equations may be expressed as

$$\frac{\partial \rho}{\partial t} + \frac{\partial \rho \boldsymbol{u}_i}{\partial \boldsymbol{x}_i} = 0, \tag{2.3}$$

$$\frac{\partial \rho \boldsymbol{u}_j}{\partial t} + \frac{\partial \rho \boldsymbol{u}_i \boldsymbol{u}_j}{\partial \boldsymbol{x}_i} = -\frac{\partial p}{\partial \boldsymbol{x}_j} + \frac{\partial \tau_{ij}}{\partial \boldsymbol{x}_i}, \tag{2.4}$$

$$\frac{\partial \rho E_t}{\partial t} + \frac{\partial \boldsymbol{u}_j (\rho E_t + p)}{\partial \boldsymbol{x}_j} = \frac{\partial \boldsymbol{u}_i \tau_{ij}}{\partial \boldsymbol{x}_j} - \frac{\partial \boldsymbol{q}_j}{\partial \boldsymbol{x}_j}, \tag{2.5}$$

and

$$\frac{\partial \rho Y_R}{\partial t} + \frac{\partial \rho \boldsymbol{u}_j Y_R}{\partial \boldsymbol{x}_j} = \frac{\partial}{\partial \boldsymbol{x}_j}\left(\frac{1}{ReSc}\mu \frac{\partial Y_R}{\partial \boldsymbol{x}_j}\right) + \dot{\omega}_R, \tag{2.6}$$

where

$$p = \frac{\gamma - 1}{\gamma}\rho T, \tag{2.7}$$

https://doi.org/10.1017/jfm.2018.115 Published online by Cambridge University Press

$$E_t = \frac{T}{\gamma} + \frac{1}{2}\boldsymbol{u}_i\boldsymbol{u}_i + \frac{\tau}{\gamma - 1}Y_R, \tag{2.8}$$

$$\tau_{ij} = \frac{\mu}{Re}\left[\frac{\partial \boldsymbol{u}_i}{\partial \boldsymbol{x}_j} + \frac{\partial \boldsymbol{u}_j}{\partial \boldsymbol{x}_i} - \frac{2}{3}\frac{\partial \boldsymbol{u}_k}{\partial \boldsymbol{x}_k}\delta_{ij}\right], \tag{2.9}$$

$$\boldsymbol{q}_j = -\frac{\mu}{Re\ Pr}\frac{\partial T}{\partial \boldsymbol{x}_j} - \frac{\mu}{Re\ Sc}\frac{\tau}{(\gamma - 1)}\frac{\partial Y_R}{\partial \boldsymbol{x}_j}, \tag{2.10}$$

and

$$\dot{\omega}_R = -Da\rho Y_R\ \exp\left[-\frac{\beta\,(1-\theta)}{1-\alpha\,(1-\theta)}\right], \tag{2.11}$$

with

$$\tau = \alpha/(1-\alpha), \quad \text{and} \quad \theta = \frac{(\gamma-1)T - 1}{\tau}. \tag{2.12a,b}$$

Note that E_t is the total energy (including sensible, kinetic and chemical energy), $\boldsymbol{q}_j$ is the heat flux vector, τ_{ij} is the ij-component of the viscous stress tensor, δ_{ij} is the Kronecker delta and $\dot{\omega}_R$ is the reactant species reaction rate. In addition, α is the heat release parameter and β is the Zel'dovich number:

$$\alpha = \frac{T_f - T_u}{T_f} \quad \text{and} \quad \beta = \frac{E_a(T_f - T_u)}{R\,T_f^2}. \tag{2.13a,b}$$

Here, T_f is the adiabatic flame temperature, T_u is the fresh (unburned) mixture temperature, E_a is the activation energy and R is the gas constant.

3. Flow configuration and numerical set-up

As shown in figure 1, a subsonic round jet of premixed reactant is injected into an open environment of combustion products at the adiabatic flame temperature. Methane/air combustion is considered at two different equivalence ratios ($\phi = 0.7$ and 1.0), with the reactants preheated to $T_u = 800$ K at 1 atm. The reactant temperature is representative of modern gas turbines. A coflow with a low velocity magnitude (1 % of the jet mean velocity) surrounds the jet flame at the inflow at the product temperature.

A simple chemistry model is used to reduce the computational cost, since the resolution required for the study of sound generation by turbulent, premixed flames is significantly higher than for non-acoustic studies of combustion (Talei *et al.* 2014). Whilst single-step chemistry is not always adequate to describe the flame structure, it can nonetheless be used to match several important parameters such as the laminar flame speed, the flame thickness, the temperature ratio and the Lewis number. The use of simple chemistry is therefore a logical first step in such studies, and is reasonably common in the literature (e.g. Haworth & Poinsot 1992; Poinsot *et al.* 1992; Chakraborty & Cant 2009; Dunstan *et al.* 2013; Karami *et al.* 2015; Chakraborty, Konstantinou & Lipatnikov 2016).

To construct the single-step chemical model, the required laminar flame speed, laminar flame thickness and adiabatic flame temperature were first obtained from PREMIX (Kee *et al.* 1985) computations with detailed chemistry using GRI-MECH 3.0 (Smith *et al.* 1999). The Zel'dovich number was also calculated following the procedure proposed by Law & Sung (2000). The values of Da_{ref} and Re_{ref} were then determined such that the values of S_L and δ_{th} calculated from a laminar, unstrained

https://doi.org/10.1017/jfm.2018.115 Published online by Cambridge University Press

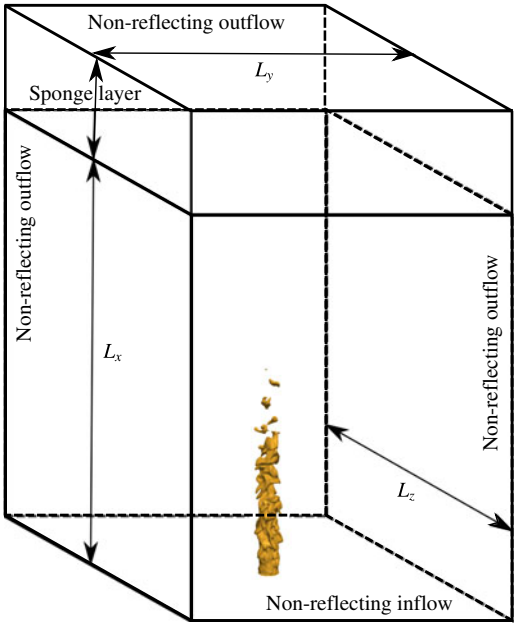


FIGURE 1. (Colour online) Schematic of the computational domain (not to scale). Note that the coordinate origin is located at the jet centreline on the inflow plane.

premixed flame simulation with simple chemistry were matched to those calculated from a PREMIX computation for each case. The computational and flame parameters are summarised in table 1. The temperature and reactant species mass fraction profiles at the inlet boundary (see figure 2*a*) were obtained using an unstrained laminar flame solution computed with the flame parameters, presented in table 1.

The mean and the root mean square (r.m.s.) profiles of the inlet streamwise velocity (see figure 2*b*) were adapted from the DNS study of Wu & Moin (2008) for a fully developed turbulent pipe flow at $Re_D = 5300$. It should be noted that the choice of Reynolds number and δ_{th}/D were constrained by the computational cost. There is a difference in the inlet Mach numbers in order to keep the Reynolds number and the normalised laminar flame thickness ($\delta_{th}/D = 0.07$) the same for both values of ϕ, as can be seen in table 1.

To impose the velocity fluctuations at the inlet, a homogeneous isotropic turbulence field based on a prescribed turbulent energy spectrum (Passot & Pouquet 1987) with a turbulence intensity of 3.7 % is first produced. (This value is equal to the turbulent intensity of the pipe flow simulation at the centreline, reported by Wu & Moin (2008).) The obtained velocity fluctuations were then rescaled using the turbulent intensity profile from Wu & Moin (2008), shown in figure 2(*b*). The resulting frozen velocity field was then added to the mean inlet velocity using Taylor's hypothesis.

The domain was resolved by a three-dimensional, structured, Cartesian mesh. A uniform grid was used in the streamwise direction. An algebraically stretched mesh with an increasing grid spacing ($(\Delta_{i+1}/\Delta_i) - 1$) not exceeding 2 % was used for $|y, z| > 1.5D$. The resulting mesh provides a uniform grid spacing with 200 grid points per jet diameter over a region covering one D on each side of the jet. This ensures that the instantaneous flame brush always remains within this finely resolved region, with 14 grid points per laminar flame thickness. Extensive mesh-independence studies

https://doi.org/10.1017/jfm.2018.115 Published online by Cambridge University Press

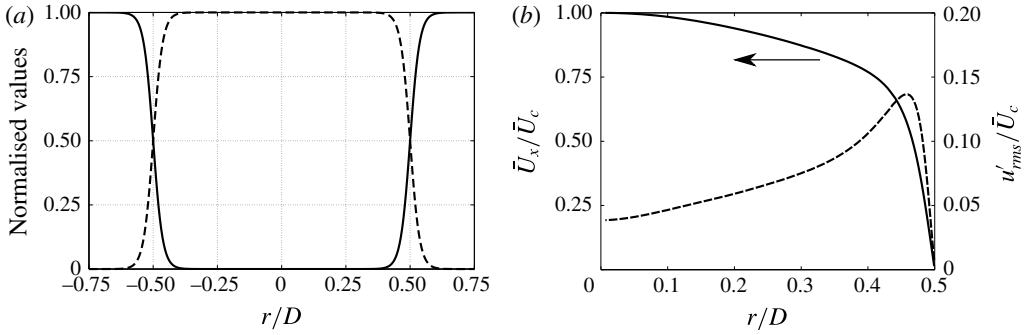


FIGURE 2. (*a*) Normalised temperature θ (solid) and reactant species mass fraction Y_R (dashed) profiles at the inlet boundary; (*b*) the mean inlet streamwise velocity ($\bar{U}_x/\bar{U}_c$) profile (solid) and the normalised r.m.s. of streamwise velocity fluctuations $u'_{rms}/\bar{U}_c$ (dashed) at the inlet boundary.

	$\phi = 1.0$	$\phi = 0.7$
Inlet jet diameter (D) in mm	3.94	4.63
Physical domain size ($L_x \times L_y \times L_z$)	$20D \times 16D \times 16D$	
Grid resolution of the physical domain	$2412 \times 1040 \times 1040$	
Sponge layer size ($L_x \times L_y \times L_z$)	$5D \times 16D \times 16D$	
Grid resolution of the sponge layer	$216 \times 1040 \times 1040$	
Mean inlet jet Mach number	0.35	0.26
Coflow Mach number	0.0035	0.0026
Heat release parameter (α)	0.675	0.637
Jet Reynolds number (Re_D)	5300	5300
Inlet centreline turbulence intensity ($u'_{rms}/\bar{U}_j$)	0.037	0.037
Kolmogorov length scale (η/D)	0.014	0.014
Karlovitz number (τ_{flame}/τ_η)	5.5	5.2
Longitudinal integral length scale (l_{11}/D)	0.30	0.30
Transverse integral length scales ($l_{22,33}/D$)	0.15	0.15
δ_{th}/D	0.07	0.07
S_L/a_{ref}	0.00422	0.00325
β	7.9	5.5
Da_{ref} (equation (2.2))	8.6	3.2
Pr	0.72	0.72

TABLE 1. DNS parameters.

were performed to ensure that the internal structure of the flame was adequately resolved and the radiated sound was free of numerical noise.

The governing equations (2.3) to (2.6) were solved using a modified version of the numerical solver S3D (Chen *et al.* 2009) known as S3D-SC (Karami *et al.* 2015, 2016, 2017). This solver features an eighth-order central differencing scheme for spatial derivatives, combined with a six-stage, fourth-order explicit Runge–Kutta time integrator. In order to suppress the spurious short waves produced by the central finite differencing scheme, a tenth-order filter is applied (Kennedy, Carpenter & Lewis 2000) at every time step.

All inflow/outflow boundaries were carefully treated to avoid spurious noise reflections. So-called standard 'Navier–Stokes characteristic boundary conditions

https://doi.org/10.1017/jfm.2018.115 Published online by Cambridge University Press

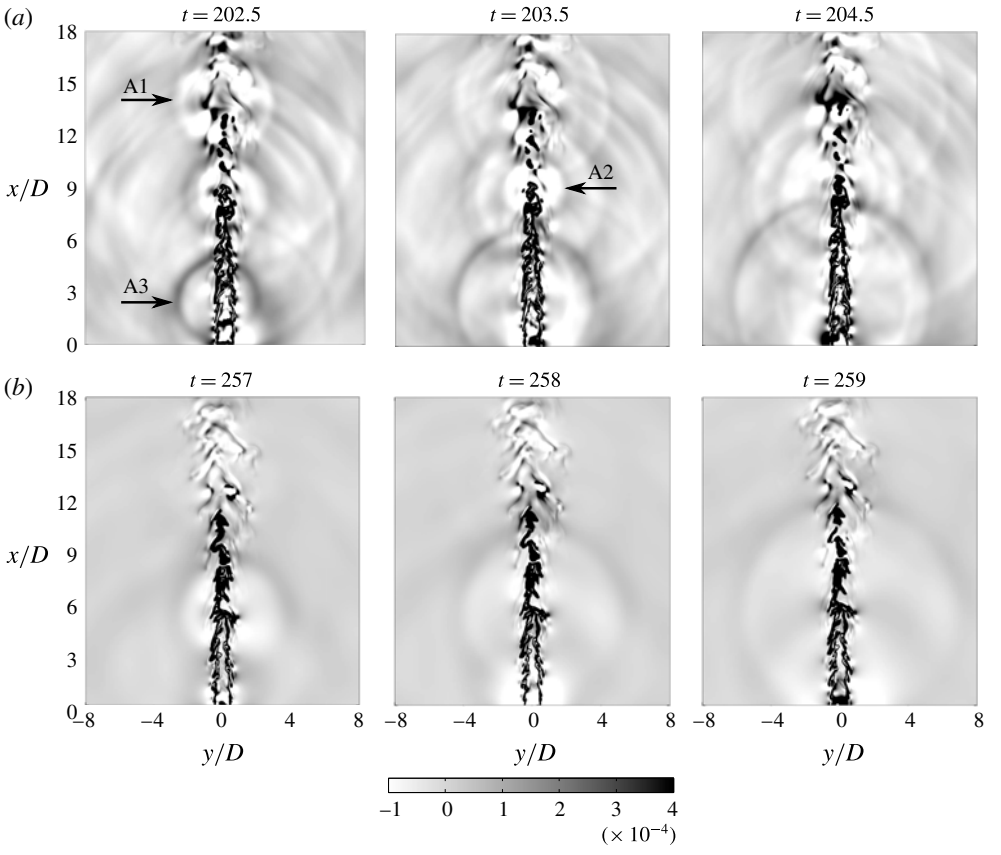


FIGURE 3. Instantaneous snapshots of the dimensionless dilatation field $\nabla \cdot \boldsymbol{u}$ on the central plane through the jet for (*a*) $\phi = 1$ and (*b*) $\phi = 0.7$.

(NSCBC)' (Poinsot & Veynante 2005) were used at the outflow planes in the transverse directions. At the inflow boundary and the streamwise outflow plane the modified NSCBC known as '3DNSCBC' (Yoo & Im 2007) were used, accounting for the effect of transverse terms. A sponge layer (Colonius, Lele & Moin 1997; Bogey, Bailly & Juvé 2000) was used for each case in the streamwise direction from $20D$ to $25D$ to gradually damp the velocity fluctuation at the outflow boundary. The sponge layer parameters were carefully chosen to ensure a negligible effect on the upstream flow field (Bogey *et al.* 2000).

The simulations were performed using a constant time step for 6 jet flow-through times $\tau_j = L_x/U_j$, and only the data from the last $4\tau_j$ were used for post-processing. The computational costs for the stoichiometric and lean cases were 1.4 and 1.9 million CPU hours respectively running on 9216 computing cores (Intel Xeon E5-2690V3 'Haswell' processors, 2.6 GHz).

4. Discussion of DNS results

4.1. *Noise sources*

Instantaneous snapshots of the dimensionless dilatation field on the central x–y plane through the jet are shown for both equivalence ratios in figure 3. (It can

https://doi.org/10.1017/jfm.2018.115 Published online by Cambridge University Press

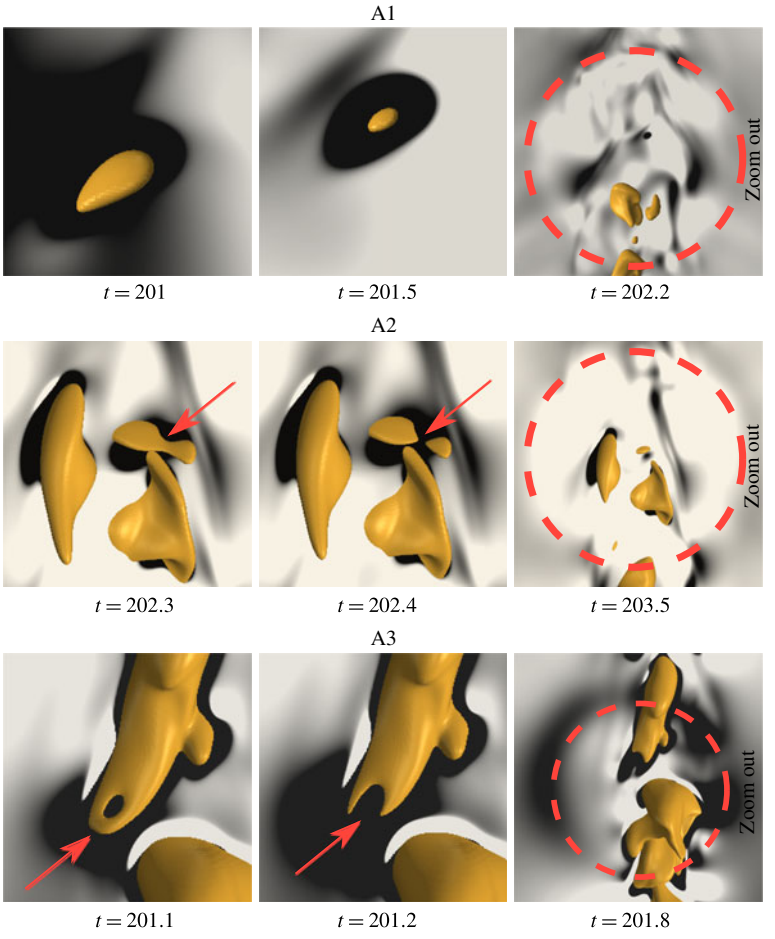


FIGURE 4. (Colour online) Instantaneous iso-surface with $Y_R = 0.122$ superimposed on the dilatation field for the three labelled events A1, A2 and A3 observed in figure 3. The dashed circle shows the monopolar sound wave generated by each annihilation event.

be readily shown that the dilatation $\nabla \cdot \boldsymbol{u}$ and the pressure are related in the far field (Colonius *et al.* 1997).) The reader is also referred to an animation of the dilatation field for these two cases in the supplementary material available at https://doi.org/10.1017/jfm.2018.115. The acoustic fields for both cases clearly feature monopolar sound sources originating from the flame. Weaker monopolar sources appear in the lean flame. Since both cases have the same Reynolds number and inlet turbulence intensities, this observation is likely related to a difference in chemical parameters between the two cases.

Figure 4 shows a flame iso-surface for events A1, A2 and A3 in figure 3 superimposed on the dilatation field. An iso-surface with $Y_R = 0.122$ for $\phi = 1.0$ is considered. This iso-surface is selected because it is close to the point of peak heat release in a one-dimensional premixed flame with the same chemistry. The event A1 involves consumption of a pocket of unburned gases in the downstream region near the flame tip. Consistent with our earlier works (Talei *et al.* 2012*b*, 2014), we refer to this phenomenon as 'flame island burn out'. Event A2 is referred to as

https://doi.org/10.1017/jfm.2018.115 Published online by Cambridge University Press

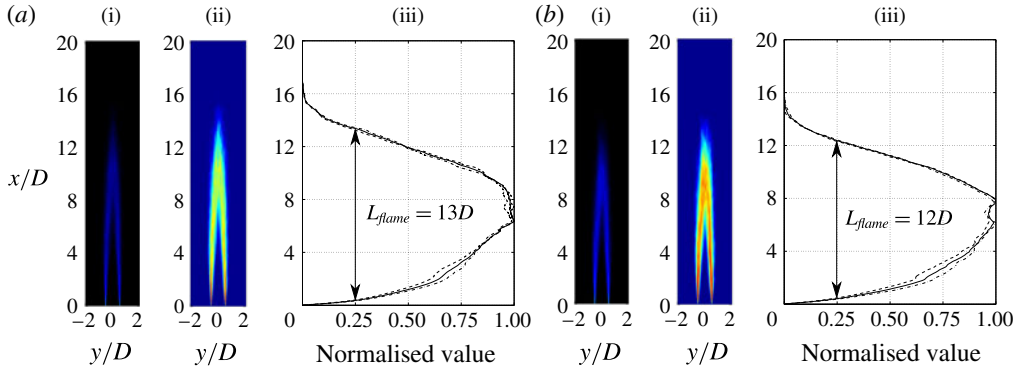


FIGURE 5. (Colour online) (i) Time-averaged reaction rate; (ii) variance of reaction rate; (iii) horizontally integrated variance field normalised by its maximum value (dashed: x–y plane, dash-dot: x–z plane and solid: the average of these planes) for (*a*) $\phi = 1.0$ and (*b*) $\phi = 0.7$.

a 'flame pinch off', with a pocket of unburned gases locally detaching from the flame surface. Finally, the event A3 takes place when flame-to-flame interaction first results in the formation of a tunnel of burned gas, and then the local flame area is lost due to cusp retraction associated with another pinch-off event. We call this first event 'tunnel formation'. All these identified events can be classified as upstream interactions since a portion of the unburned gas is consumed by propagation of flame surfaces (Chen & Sohrab 1995). The topology of these events has been studied by Dunstan *et al.* (2013) and more recently by Griffiths *et al.* (2015). Figure 3 suggests that these frequent flame annihilation events play an important role in the generation of sound.

4.2. *Spectral analysis*

Rajaram & Lieuwen (2009) showed that a peak Strouhal number $St_{peak} = f_{peak} L_{flame}/U_{av}$ of the far-field spectrum was always of order unity and varied between 0.5 and 2.2 across a large set of turbulent premixed flames tested, where L_{flame} was a flame length and U_{av} was the cold flow, bulk jet velocity. It should, however, be noted that Rajaram & Lieuwen (2009) calculated their flame length using the variance in the intensity of chemiluminescence emitted by the flame at a given point in space. The flame length (L_{flame}) was then defined as the distance between the heights where the horizontally integrated intensity of the variance image crosses a quarter of its maximum value. In the present study, the flame length was therefore calculated using the variance of the reaction rate field. As depicted in figure 5, these flame lengths were approximately equal to $13D$ and $12D$ for the stoichiometric and lean cases, respectively. The spectrum of the produced sound is calculated on a plane perpendicular to the jet axis at $x = 10D$ using thirty two virtual microphones that were uniformly distributed at $r = 6D$. To reduce the so-called 'spectral leakage', a modified Hanning window (Lockard 2000) with 50 % overlap (Bui *et al.* 2008) was used to perform the fast Fourier transform (FFT) at each probe. The data for $\phi = 1$ and 0.7 cases were collected for 1.43 and 2.9 ms. Since we have used a Hanning window with 50 % overlap, the lowest frequency that we can capture from the DNS is then approximately 1 kHz. This computational study is already very resource intensive, it is therefore impractical to reduce this lower frequency bound significantly, as this requires a corresponding increase in the computational cost.

https://doi.org/10.1017/jfm.2018.115 Published online by Cambridge University Press

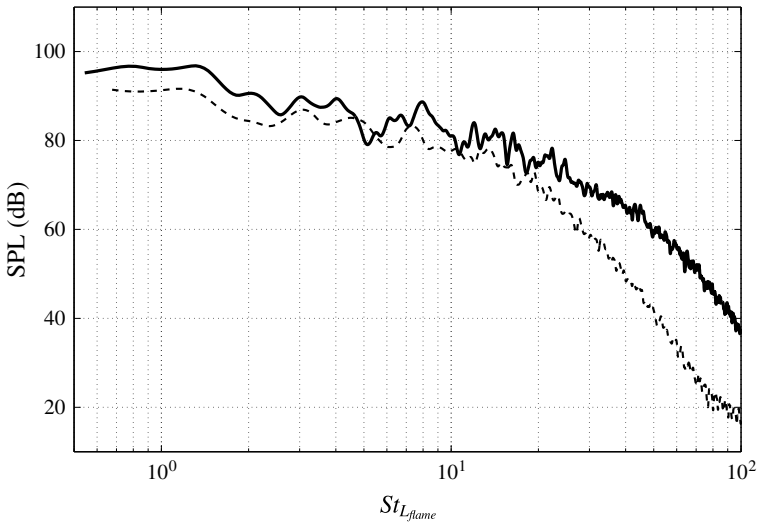


FIGURE 6. Noise spectrum for $\phi = 1.0$ (solid) and $\phi = 0.7$ (dashed) considering 32 equally spaced probes at $x/D = 10$ and $r/D = 6$. The horizontal axis shows Strouhal number based on flame length ($St_{L_{flame}} = fL_{flame}/U_{av}$). The vertical axis shows the sound pressure level (SPL) in dB.

The averaged spectrum for both cases is shown in figure 6. The magnitude of the noise radiated by the stoichiometric flame is greater than that of the lean flame. This is examined later in this section. Using the calculated flame lengths, the peak Strouhal numbers for the stoichiometric and lean flames are 1.3 and 1.2, respectively, which fall within the range found experimentally by Rajaram & Lieuwen (2009).

However, Rajaram & Lieuwen (2009) also observed that the high frequency spectra rolls off at 42–64 (dB/decade) across $St_{L_{flame}} \sim 1$–100 for several different flames with $Re_D > 10^4$. This is not observed in the present study. There are several potential reasons for this observed difference. Those expected to be of particular significance are the two studies' differing inflow turbulence, differing forms of flame stabilisation, and the present study's lower jet Reynolds number of $Re_D \sim 5000$.

It is also worth mentioning that our DNS is undertaken at significantly different conditions to experimental studies such as Rajaram & Lieuwen (2009). The same range of frequencies for DNS and experiment should therefore not be expected. Nonetheless, our captured range of frequencies non-dimensionalised by the frequency of peak emission is approximately between 0.4 and 100, which is in agreement with the range observed by Rajaram & Lieuwen (2009) for natural gas (the relevant fuel to our study).

To shed light on the reason for the stoichiometric flame being louder than the lean flame, the scaling analysis performed by Rajaram, Gray & Lieuwen (2006) is extended here. In this scaling, the total acoustic power, P, is considered to be proportional to $(\mathrm{d}Q/\mathrm{d}t)^2$. The underlying assumption is the heat release rate fluctuations, $\mathrm{d}Q/\mathrm{d}t$, being the dominant source of noise, as discussed in § 1. The following scaling can then be derived:

$$\frac{\mathrm{d}Q}{\mathrm{d}t} \sim \frac{Q_{char}}{t_{char}}, \tag{4.1}$$

https://doi.org/10.1017/jfm.2018.115 Published online by Cambridge University Press

where Q_{char} is the characteristic heat release rate estimated by $\dot{m}c_p(T_b - T_u)$ and t_{char} is the characteristic time scale estimated by $1/f_{peak}$. Rajaram & Lieuwen (2009) showed that the frequency of peak emission can be scaled with U/L_{flame}. This is analogous to the scaling performed for non-reacting jets, in which the relevant frequency for sound generation is estimated as U/D (Dowling & Ffowcs Williams 1983). Considering a premixed flame as a monopolar source of noise, it is reasonable to assume that the relevant length scale is the averaged flame length. These assumptions then lead to:

$$\frac{\mathrm{d}Q}{\mathrm{d}t} \sim \rho_u U D^2 c_p (T_b - T_u) f_{peak} \sim \rho_u c_p (T_b - T_u) U^2 D^2 / L_{flame}. \tag{4.2}$$

The averaged flame length can be then estimated by assuming a small flame cone angle using the following expressions:

$$L_{flame} \sim UD/S_T, \tag{4.3}$$

where S_T is the averaged turbulent flame speed. According to the resent work by Fogla, Creta & Matalon (2017), S_T can be generally described as,

$$S_T = S_L f(T_b/T_u, u'/S_L, l_T/D, \mathscr{M}), \tag{4.4}$$

where l_T is the turbulence integral length scale and $\mathscr{M}$ is the Markstein number. The total acoustic power can then be estimated as:

$$P \sim \rho_u^2 c_p^2 T_u^2 (UDS_L)^2 (T_b/T_u - 1)^2 f^2 (T_b/T_u, u'/S_L, l_T/D, \mathscr{M}). \tag{4.5}$$

It is interesting to note that the term $(UDS_L)^2$ which is an empirical correlation proposed by Smith & Kilham (1963) appears in (4.5). This equation can be further rearranged to

$$P \sim \rho_u^2 c_p^2 \nu^2 T_u^2 S_L^2 Re_D^2 (T_b/T_u - 1)^2 f^2 (T_b/T_u, u'/S_L, l_T/D, \mathscr{M}). \tag{4.6}$$

The jets in our study feature the same jet Reynolds number, turbulence intensity ($u'/S_L \sim 3$) and turbulence length scale at the inlet (cf. table 1). For unity Lewis number, the Markstein number $\mathscr{M}$ is a function of temperature ratio only (Clavin & Joulin 1983) which leads to a slightly higher value for the stoichiometric case. Equation (4.6) therefore states that the higher flame speed and the higher temperature ratio of the stoichiometric flame play an important role in determining why the stoichiometric flame is louder than the lean flame.

4.3. *Identification of flame annihilation*

We have argued that flame annihilation events play a significant role in the noise generated by a turbulent premixed flame. A means of identifying these events should therefore be defined. It is known that flames accelerate prior to flame annihilation (e.g. Echekki *et al.* 1996; Sun & Law 1998). The impact of this acceleration on the produced sound was also discussed by Talei *et al.* (2011). To capture this acceleration, the density-weighted displacement speed of the flame relative to the local gas velocity (Echekki & Chen 1999) is therefore considered in non-dimensional form,

$$S_d^* \equiv \frac{\rho S_d}{\rho_u} = -\frac{\dot{\omega}_R}{\rho_u |\nabla Y_R|} - \frac{1}{Sc\, Re} \frac{\boldsymbol{n} \cdot \nabla(\mu |\nabla Y_R|)}{\rho_u |\nabla Y_R|} - \frac{\mu}{Sc\, Re\, \rho_u} (\nabla \cdot \boldsymbol{n}). \tag{4.7}$$

The density-weighted form of the flame displacement is used since this minimises the effect of thermal expansion on the displacement speed. Here, $(\nabla \cdot \boldsymbol{n})$ is the flame

https://doi.org/10.1017/jfm.2018.115 Published online by Cambridge University Press

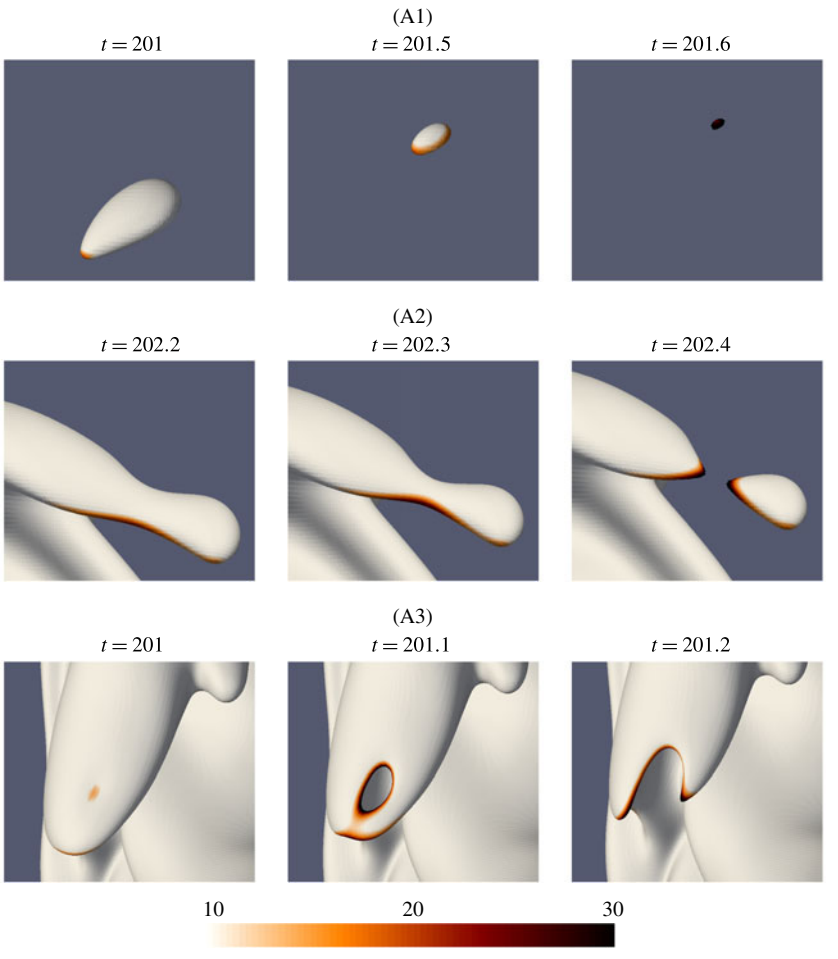


FIGURE 7. (Colour online) The time evolution of the three flame annihilation events labelled in figure 3 and their corresponding normalised density-weighted flame displacement speed (S_d^*/S_L) fields mapped on the flame surface.

curvature where $\boldsymbol{n}$ is the unit normal vector of the iso-contour of Y_R directed towards the reactant,

$$\boldsymbol{n} = \frac{\nabla Y_R}{|\nabla Y_R|}. \tag{4.8}$$

The flame curvature is taken to be negative (positive) when the flame is curved towards the fresh reactant (burned mixture). Note that (4.7) shows that the flame displacement speed is obtained by the relative contributions of the reaction rate, the normal diffusion and the flame curvature.

Figure 7 illustrates the iso-surface of the progress variable $Y_R = 0.122$ corresponding to the three distinct flame annihilation events A1 to A3 in figure 3. These iso-surfaces are now coloured with the normalised density-weighted flame displacement speed (S_d^*/S_L). There is a large increase in the magnitude of S_d^*/S_L during the annihilation events. Thus, $S_d^*/S_L > 10$ seems to be a reasonable condition for identifying annihilation events.

https://doi.org/10.1017/jfm.2018.115 Published online by Cambridge University Press

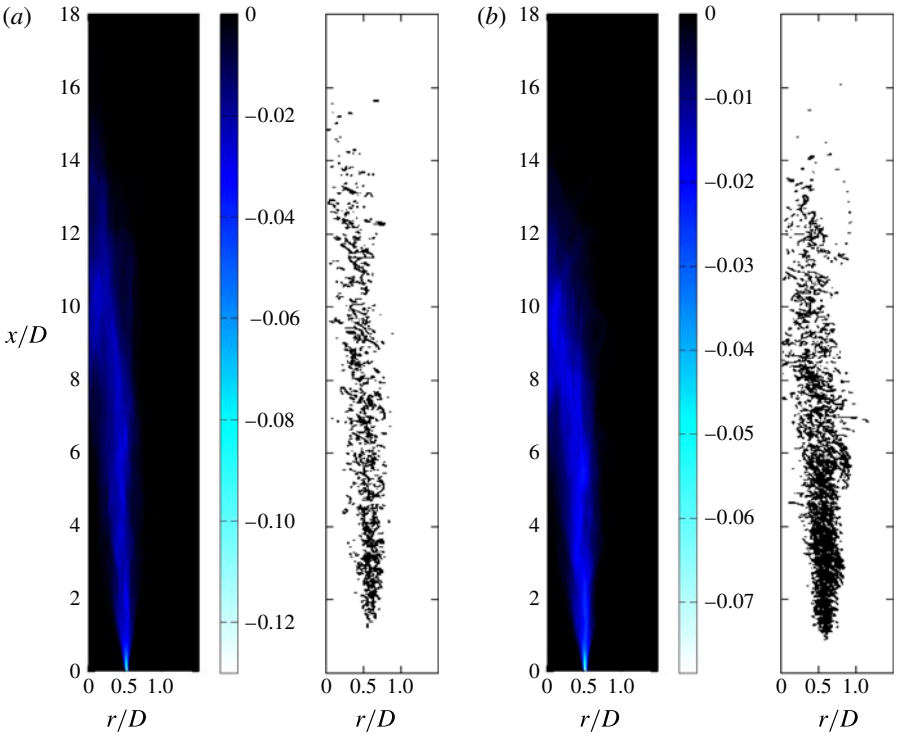


FIGURE 8. (Colour online) Time-averaged reaction rate and instantaneous scatter plot of nodes with $S_d^*/S_L > 10$ on an iso-surface with (*a*) $Y_R = 0.122$ for $\phi = 1.0$ and (*b*) $Y_R = 0.156$ for $\phi = 0.7$.

Figure 8 therefore shows scatter plots of grid nodes that satisfy this proposed identifier of flame annihilation, i.e. points with $Y_R = 0.122$ for $\phi = 1.0$ ($Y_R = 0.156$ for $\phi = 0.7$) and $S_d^*/S_L > 10$. These scatter plots were generated using the same time period, which was the flow through time of the stoichiometric case detailed in table 1. Events throughout the stoichiometric and lean flames are evident and common. Perhaps surprisingly, the lean flame shows more of these events even though figures 3 and 6 showed that it was the quieter flame. However, this is not necessarily a contradiction, particularly since premixed flame noise is known to scale with the laminar flame speed (Smith & Kilham 1963; Strahle & Shivashankara 1975; Talei *et al.* 2011). We therefore now consider how identification of these events can be used in a simple model of the radiated sound.

5. A simple model of sound generation by flame annihilation

We now consider a simple model of sound generation by these annihilation events. This model is consistent with the approach of Smith & Kilham (1963), and considers the flame to be a distribution of annihilation events, each of which radiates monopolar sound to the far field. This simple model is therefore only a means of assessing the contribution of annihilation events to the overall sound produced by turbulent premixed flames, and is not intended to be a complete model of sound production since other sources are neglected.

https://doi.org/10.1017/jfm.2018.115 Published online by Cambridge University Press

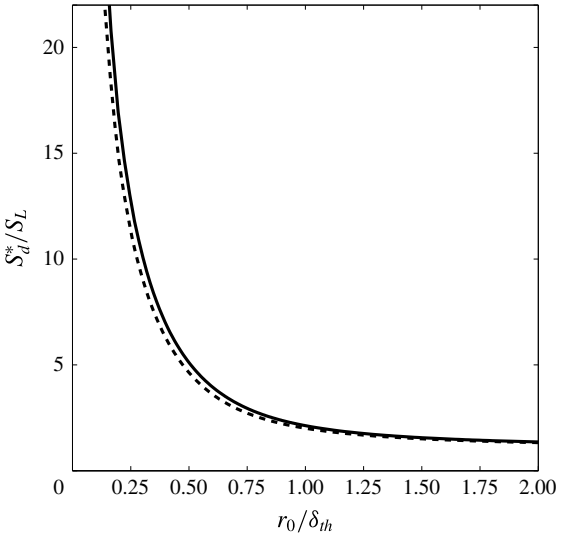


FIGURE 9. Normalised density-weighted flame displacement speed (S_d^*/S_L) as a function of normalised flame radius (r_0/δ_{th}) for a spherically symmetric annihilation event for $\phi = 1.0$ (solid) and $\phi = 0.7$ (dashed).

5.1. *Laminar flame annihilation*

Spherically symmetric annihilation events are simulated first. The flame parameters are the same as those used in the turbulent flames for both stoichiometric and lean conditions. After initialising the flow field, the spherical flames start to propagate from their initial position at $r_0/\delta_{th} = 7$, where r_0 is the distance from the origin.

Figure 9 shows S_d^*/S_L as a function of r_0/δ_{th} for both cases. It is observed that S_d^*/S_L has a value of approximately unity when the flame is at $r_0/\delta_{th} \approx 2$. After that, S_d^*/S_L starts to increase, reaching very large values during annihilation, as several other studies have found (e.g. Echekki *et al.* 1996; Sun & Law 1998).

Figure 10 shows a comparison of the sound produced by both annihilation events at $r/\delta_{th} = 28$, where r is the distance between the receiver and the centre of the flame sphere. The annihilation event corresponding to the lean flame is much quieter than that of the stoichiometric flame. This is consistent with Talei *et al.* (2011), who found that the sound produced for a spherically symmetric annihilation event is proportional to S_L^2. This can also likely contribute to the lower level of noise produced by the turbulent lean flame.

5.2. *Theory*

Talei *et al.* (2012*a*) used the theory of Dowling (1992), which in turn extended Lighthill's equation (Lighthill 1952, 1954), for the study of combusting flows. By considering the fluctuations in heat release as the only source term, modelling the reaction rate as a delta function and assuming a constant consumption speed, Talei *et al.* (2012*a*) showed that the general solution of Lighthill's equation for a spherically symmetric annihilation event is

$$p'(r, t) = -2\rho_u S_L \left(1 - \frac{T_u}{T_b}\right) \frac{r_0(t - r/c_b)}{r} V_f(t - r/c_b) H(t - r/c_b), \tag{5.1}$$

https://doi.org/10.1017/jfm.2018.115 Published online by Cambridge University Press

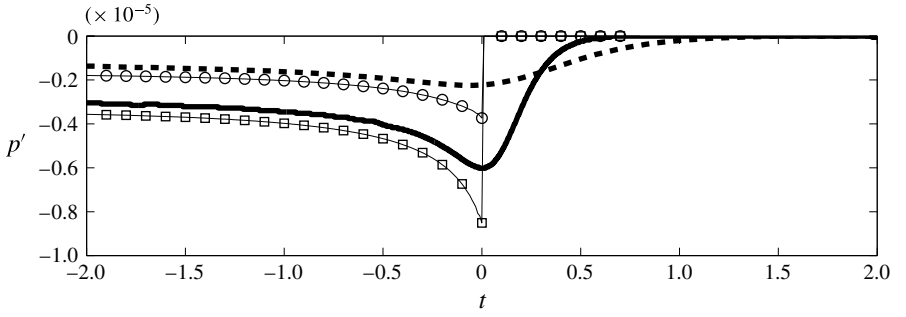


FIGURE 10. Time history of sound generated by a spherically symmetric annihilation event at $r/\delta_{th} = 28$ from DNS for $\phi = 1.0$ (solid) and $\phi = 0.7$ (dashed) and by (5.1) for $\phi = 1.0$ (square) and $\phi = 0.7$ (circle).

where p' is the fluctuating part of the pressure, c_b is the burned sonic speed, H is the Heaviside function and V_f is the magnitude of flame propagation velocity $\boldsymbol{V}_f$ projected onto the flame normal $\boldsymbol{n}$,

$$V_f \equiv \boldsymbol{V}_f \cdot \boldsymbol{n} = \boldsymbol{u} \cdot \boldsymbol{n} + S_d. \tag{5.2}$$

Figure 10 compares p' from DNS and (5.1) for spherical annihilation events. The over-prediction of the peak pressure is due to the assumption of constant consumption speed, particularly at the later stages of the annihilation event (Talei *et al.* 2012*a*). The step at the peak acoustic pressure in the theory is because the flame is represented as a delta function.

5.3. *Model for turbulent premixed flames*

5.3.1. *Model description*

Equation (5.1) provides a reasonable model of the noise generated by a single spherical annihilation event. However, this theory now needs to be extended to estimate sound generation by the various types of annihilation that occur throughout a turbulent flame. A precise extension of this equation to different types of annihilation events involves a substantial numerical and theoretical study to construct a model which incorporates the features of different types of annihilation events. This is beyond the scope of this work. Thus, as a first step, all annihilation events are assumed to be spherically symmetric, and the simplification in making this assumption must always be kept in mind.

The iso-surface of the progress variable corresponding to the maximum reaction rate ($Y_R = 0.122$ and 0.156 for $\phi = 1.0$ and $\phi = 0.7$ respectively) are then conditioned using $S_d^*/S_L \geqslant n$ as a marker. Figure 11 shows the effect of different values of n on the noise generated by a spherically symmetric annihilation event using a modified form of (5.1),

$$\begin{aligned} p'(r,t) \;=\; & -2\rho_u S_L \left(1 - \frac{T_u}{T_b}\right) \frac{r_0(t - r/c_b)}{r} V_f(t - r/c_b) \\ & \times H(t - r/c_b) H\left(\frac{S_d^*(t - r/c_b)}{S_L} - n\right). \end{aligned} \tag{5.3}$$

https://doi.org/10.1017/jfm.2018.115 Published online by Cambridge University Press

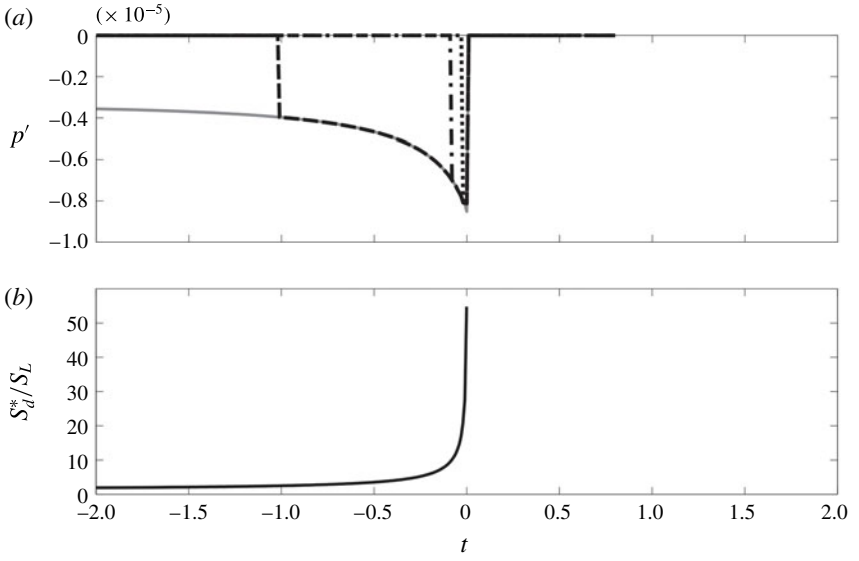


FIGURE 11. (*a*) Comparison of the sound generated by a spherically symmetric annihilation event at $r/\delta_{th} = 28$ using (5.1) (solid) and the modified theory (equation (5.3)) with $n = 2.5$ (dashed), 10 (dash-dot) and 20 (dotted). (*b*) The corresponding time history of S_d^*/S_L for this event.

The rightmost Heaviside function in (5.3) is added to capture annihilation events. As mentioned earlier, flame acceleration is a defining feature of these events. We therefore use this function to identify annihilation by setting a threshold on $S_d^*/S_L = n$. It can be seen that when $n = 2.5$ is chosen, the whole annihilation is captured whereas for $n = 20$, only the final stage of annihilation is recovered. Equation (5.3) requires the information at $t - r/c_b$ for each annihilation event. This instant might not coincide with the instants at which the DNS data are collected. We therefore used a time shift r/c_b to obtain the pressure fluctuations at a later time as follows:

$$p'(r, \tau + r/c_b) = -2\rho_u S_L \left(1 - \frac{T_u}{T_b}\right) \frac{r_0(\tau)}{r} V_f(\tau) H\left(\frac{S_d^*(\tau)}{S_L} - n\right), \tag{5.4}$$

where $\tau = t - r/c_b$ and r_0 is determined from figure 9 at a given S_d^*/S_L.

5.3.2. *Algorithm*

There are four steps in our modelling algorithm.

(i) Divide the domain into cubes.
(ii) Identify flame annihilation events.
(iii) Represent the flame with a number of spherically symmetric annihilation events.
(iv) Calculate the total sound produced.

Figure 9 shows that having information from the instant at which $r_0 = \delta_{th}$ is sufficient to represent the annihilation event. Note that $r_0 = \delta_{th}$ corresponds to $S_d^*/S_L \approx 2.5$ which is the lowest threshold for S_d^*/S_L considered in this study. We therefore assume that each cube in the domain has a size of $2\delta_{th}$ in which only one spherically symmetric annihilation event can occur at any time. The entire domain

https://doi.org/10.1017/jfm.2018.115 Published online by Cambridge University Press

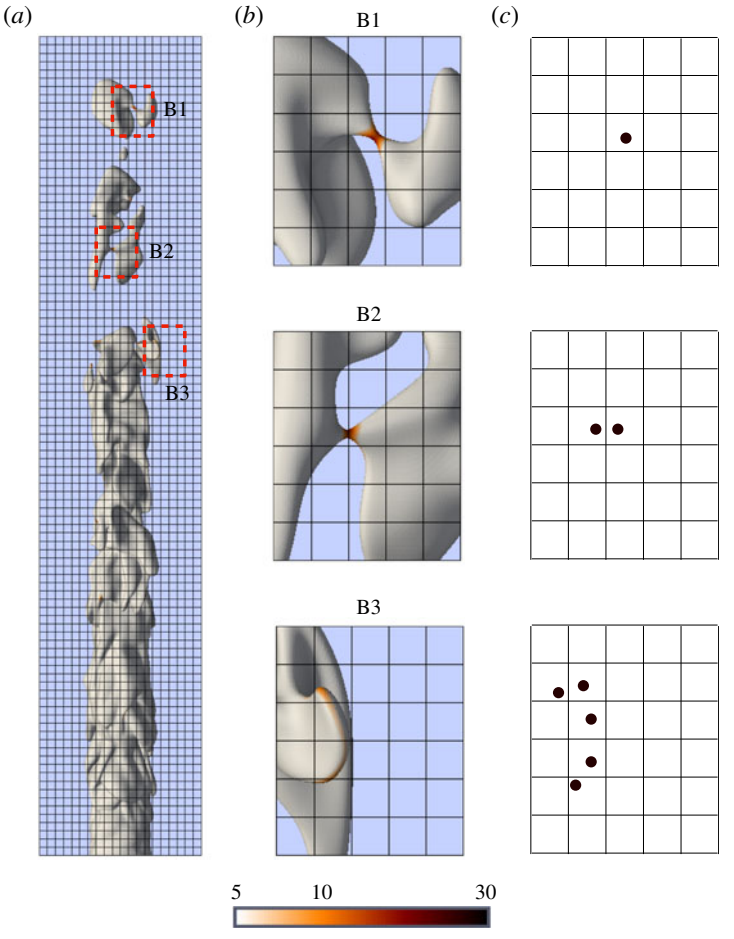


FIGURE 12. (Colour online) (*a*) One snapshot of the flame iso-surface for $\phi = 1.0$ on a uniform mesh with a cube of edge length $\Delta = 2\delta_{th}$. (*b*) The regions B1, B2 and B3 in (*a*) are zoomed in and coloured with the S_d^*/S_L field. (*c*) Centroid of the cluster of the conditioned data as per § 5.3.2.

that features the flame is therefore divided into these uniformly distributed cubes (figure 12*a*).

For step 2, the points on the iso-surfaces of Y_R (0.122 and 0.156 for the stoichiometric and the lean cases, respectively) in each cube with $S_d^*/S_L \geqslant n$ and $V_f > 0$ are identified at each instant. Figure 12(*b*) shows examples of the identified points for different types of annihilation events.

For step 3, the cluster of points in each cube is now replaced with one point at the centroid of the cluster with an averaged propagation velocity obtained from the velocity of each point. This point is considered as one spherically symmetric annihilation event. Figure 12(*c*) shows how the flame pinch-off event labelled as B1 is represented by one spherically symmetric annihilation. Another flame pinch-off event labelled as B2 is considered as two events since it is split into two cubes. Although this event is very similar to that labelled as B1, it will be modelled as a sound source of twice the strength. This is an unavoidable and undesirable feature of

https://doi.org/10.1017/jfm.2018.115 Published online by Cambridge University Press

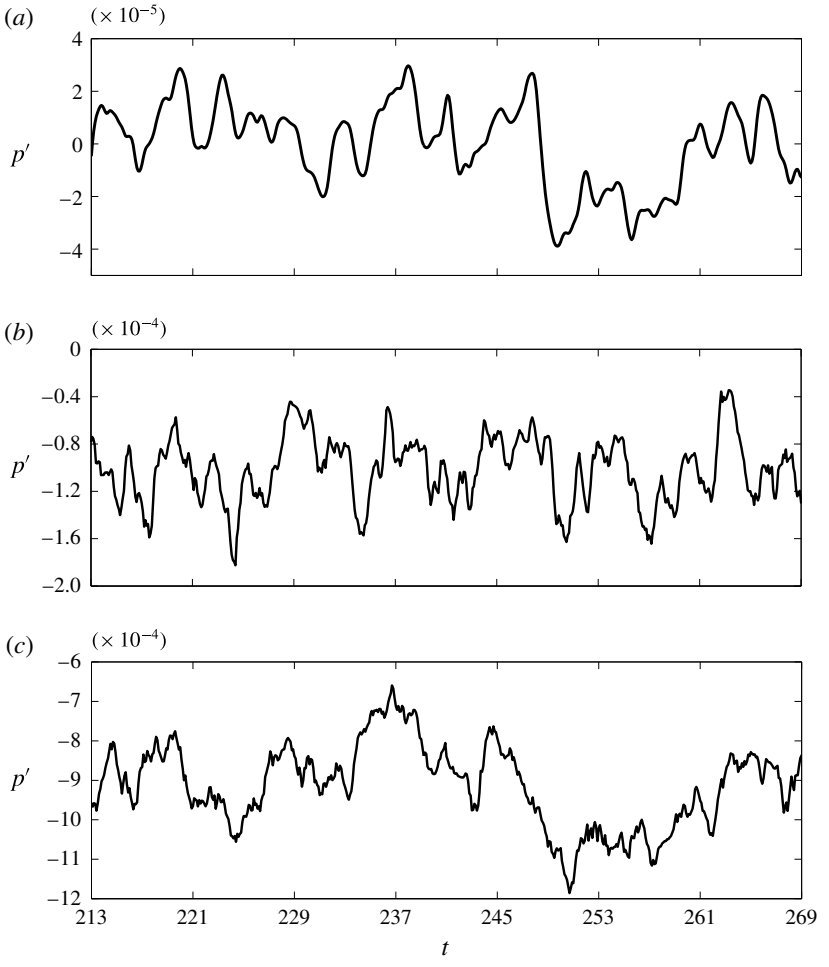


FIGURE 13. Time history of the far-field noise at $r = 6D$ and $x = 10D$ for $\phi = 1.0$, obtained from (*a*) DNS, (*b*) model with $n = 10$ and (*c*) model with $n = 5$.

this algorithm, with some over-prediction of the sound expected to result. Finally, the event labelled as B3 shows a long, curved flame edge distributed over several cubes. Once again, this will potentially contribute to over-prediction of the sound.

Step 4 then calculates the overall sound produced by calculating the noise generated by each annihilation event. First, a number of time bins (with the bin size equal to the sampling size of the DNS data) are considered and the result of (5.4) for each representative point source is stored in its associated time bin. Then, p' in the far field resulting from the sound produced by all points is calculated by summing the stored values in each time bin.

5.4. *Comparison of the simple model with DNS*

Figure 13(*a*) depicts the time history of the acoustic pressure p' at $x = 10D$ and $r = 6D$ (One should note that since the relevant length scale for annihilation events is the flame thickness, the receiver $r = 85\delta_{th}$ is sufficiently far from the jet to be considered in the far field, as our previous studies of laminar flames have shown

https://doi.org/10.1017/jfm.2018.115 Published online by Cambridge University Press

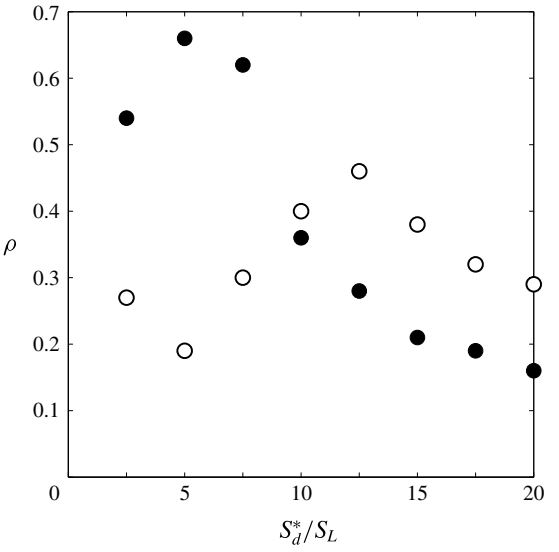


FIGURE 14. Correlation coefficient ρ between the DNS far-field noise and that of the model at $r = 6D$ and $x = 10D$ as a function of S_d^*/S_L for $\phi = 1$ (solid circles) and $\phi = 0.7$ (hollow circles).

(Talei *et al.* 2011, 2012*a*).) obtained from the DNS for the case with $\phi = 1.0$. Figure 13(*b*,*c*) shows the corresponding model results for $n = 10$ and 5, respectively. The modelled signals contain some high frequency noise which is due to the model representing the flame as discrete point sources that appear and disappear rapidly due to the conditioning on S_d^*/S_L. The correlation coefficient, $\rho = \mathrm{cov}(X, Y)/(\sigma(X)\sigma(Y))$, between the modelled signal and the DNS data is 36 % for $n = 10$ and 66 % when $n = 5$ is used. A comparison of figures 13(*b*,*c*) and 13(*a*) also shows that the magnitude of the pressure fluctuations is over-predicted by the model, as discussed in § 5.3.2. Clearly, the choice of threshold n is important.

A range of n from 2.5 to 20 is therefore considered. For high values of n, some of the annihilation events are not captured because of the finite time resolution of the recorded DNS data. On the other hand, choosing a low value of n will include parts of the flame surface which are not annihilation events. This suggests that there will be an optimum value of n in terms of correlation coefficient. Figure 14 supports this hypothesis by showing that $n = 5$ and $n = 12.5$ are optimal for the stoichiometric and lean cases, respectively. The optimal correlation is particularly strong for the stoichiometric flame, demonstrating the significant contribution of annihilation events to sound production.

Figure 15 shows this correlation coefficient over an x–z plane located at $y/D = -6$. The optimum values of n for both flames in figure 14 are used to calculate the correlation coefficient. While an almost uniform distribution is observed for the stoichiometric flame (figure 15*a*), two distinct zones are found for the lean flame (figure 15*b*). This shows that annihilation events are a strong source of noise for the stoichiometric flame. There is, however, a competition between the sound produced by the annihilation events and other sources such as the inflow noise for the quieter, lean flame.

The degree of correlation between the DNS and the model in figure 15 is surprising given the model's simplicity. The model considers all sound sources to be spherically

https://doi.org/10.1017/jfm.2018.115 Published online by Cambridge University Press

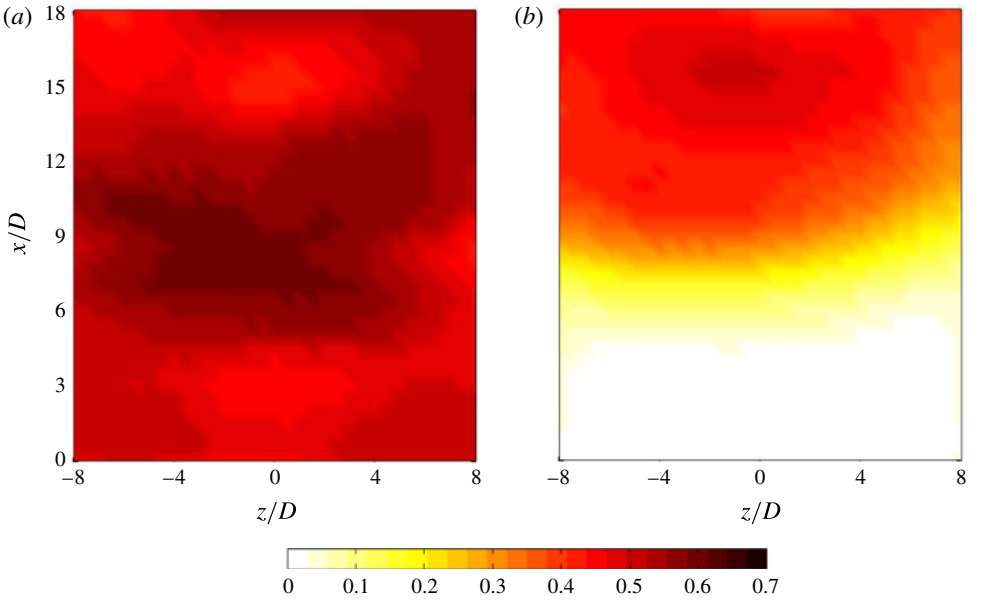


FIGURE 15. (Colour online) Distribution of the correlation coefficient ρ between the DNS and the model calculated over an x–z plane located at $y/D = -6$ for (*a*) $\phi = 1.0$ with $n = 5$ and (*b*) $\phi = 0.7$ with $n = 12.5$.

symmetric annihilations, even though other forms of annihilation were shown to exist and other sound sources are expected in combusting flows (Dowling 1992; Talei *et al.* 2014). Further, all sound is modelled as travelling radially from these sources at the burnt gas velocity, ignoring refraction and sound propagation at lower velocity, as should occur for a source on one side of the flame with the receiver on the other side.

Smith & Kilham's (1963) model of a flame as a distribution of monopolar sound sources therefore appears to be insightful. The simple model in the present work identifies flame annihilation events as these sources and, in so doing, provides a physical explanation for the well-known monopolar content of the sound radiated by premixed turbulent flames.

6. Conclusions

This paper presented a numerical study of the sound generated by turbulent, premixed flames. Direct numerical simulations (DNS) of two round jet flames with equivalence ratios of 0.7 and 1.0 were first carried out. Single-step chemistry was employed to reduce the computational cost, and care was taken to resolve both the near and far fields and to avoid noise reflections at the outflow boundaries.

Several significant features of these two simulated flames were noted. First, the acoustic fields of both the stoichiometric and lean flames exhibited monopolar features that originated within the flame, with the stoichiometric flame being significantly louder than the lean flame. These observations are consistent with several experimental studies of turbulent jet flames in the literature. Further, so-called 'flame annihilation' events were observed to be a source of these monopolar, acoustic features, which was consistent with prior works on laminar premixed flames. The acoustic spectra of

https://doi.org/10.1017/jfm.2018.115 Published online by Cambridge University Press

both flames were also studied. These were found to be broadband in nature, with a frequency at the peak spectral amplitude agreeing with those observed experimentally by Rajaram & Lieuwen (2009).

A simple model that related the observed annihilation events to the far-field sound was then proposed. This model considered the far-field sound as the superposition of the sound radiated by individual, spherically symmetric annihilation events that occurred throughout the flame. These events were identified by conditioning the flame displacement speed at some threshold since flame annihilation is well known to feature flame acceleration. The choice of threshold was shown to strongly affect the correlation between the modelled and measured, far-field sound, with the correlation coefficient exceeding 0.5 in some cases. Such levels of correlation were surprising given the model's simplicity, and demonstrated the importance of flame annihilation as acoustic sources in turbulent premixed flames. This model is also consistent with Smith & Kilham's (1963) model of a flame as a distribution of monopolar sound sources, with the present work identifying flame annihilation events as these sources and, in so doing, providing a physical explanation for the well-known monopolar content of the sound radiated by premixed turbulent flames.

Acknowledgements

This study was supported by the Advanced Centre for Automotive Research and Testing (ACART, www.acart.com.au), the Australian Research Council (ARC) and the Australian Government's National Computational Merit Allocation Scheme. The computational facilities supporting this project included the Australian National Facility (NCI), the partner share of the NCI facility provided by Intersect Australia Pty Ltd. and the Pawsey Supercomputing Centre.

Supplementary material

Supplementary material is available at https://doi.org/10.1017/jfm.2018.115.

REFERENCES

BALACHANDRAN, R., AYOOLA, B. O., KAMINSKI, C. F., DOWLING, A. P. & MASTORAKOS, E. 2005 Experimental investigation of the nonlinear response of turbulent premixed flames to imposed inlet velocity oscillations. *Combust. Flame* **143** (1), 37–55.

BIRBAUD, A. L., DUCRUIX, S., DUROX, D. & CANDEL, S. 2006 Dynamics of free jets modulated by plane acoustic waves: part 2. Numerical simulations. In *12th AIAA/CEAS Aeroacoustics Conference (27th AIAA Aeroacoustics Conference), Cambridge, MA, AIAA Paper* 2006-2670.

BOGEY, C., BAILLY, C. & JUVÉ, D. 2000 Numerical simulation of sound generated by vortex pairing in a mixing layer. *AIAA J.* **38** (12), 2210–2218.

BRAGG, S. L. 1963 Combustion noise. *J. Inst. Fuel* **36** (1), 12–16.

BREAR, M. J., NICOUD, F., TALEI, M., GIAUQUE, A. & HAWKES, E. R. 2012 Disturbance energy transport and sound production in gaseous combustion. *J. Fluid Mech.* **707**, 53–73.

BUI, T. P., IHME, M., SCHRÖDER, W. & PITSCH, H. 2009 Analysis of different sound source formulations to simulate combustion generated noise using a hybrid LES/APE-RF method. *Intl J. Aeroacoust.* **8** (1), 95–123.

BUI, T. P., MEINKE, M., SCHRÖDER, W., FLEMMING, F., SADIKI, A. & JANICKA, J. 2005 A hybrid method for combustion noise based on LES and APE. *AIAA Paper* 2005-3014.

BUI, T. P., SCHRÖDER, W. & MEINKE, M. 2008 Numerical analysis of the acoustic field of reacting flows via acoustic perturbation equations. *Comput. Fluids* **37** (9), 1157–1169.

https://doi.org/10.1017/jfm.2018.115 Published online by Cambridge University Press

CANDEL, S., DUROX, D. & SCHULLER, T. 2004 Flame interactions as a source of noise and combustion instabilities. In *Collection of Technical Papers-10th AIAA/CEAS Aeroacoustics Conference*, *AIAA Paper* 2004-2928, pp. 1444–1454.

CHAKRABORTY, N. & CANT, R. S. 2009 Direct numerical simulation analysis of the flame surface density transport equation in the context of large eddy simulation. *Proc. Combust. Inst.* **32** (1), 1445–1453.

CHAKRABORTY, N., KONSTANTINOU, I. & LIPATNIKOV, A. 2016 Effects of Lewis number on vorticity and enstrophy transport in turbulent premixed flames. *Phys. Fluids* **28** (1), 015109.

CHEN, C. L. & SOHRAB, S. H. 1995 Upstream interactions between planar symmetric laminar methane premixed flames. *Combust. Flame* **101** (3), 360–370.

CHEN, J. H., CHOUDHARY, A., DE SUPINSKI, B., DEVRIES, M, HAWKES, E. R., KLASKY, S., LIAO, W. K., MA, K. L., MELLOR-CRUMMEY, J., PODHORSZKI, N. *et al.* 2009 Terascale direct numerical simulations of turbulent combustion using S3D. *Comput. Sci. Disc.* **2** (1), 015001.

CLAVIN, P. & JOULIN, G. 1983 Premixed flames in large scale and high intensity turbulent flow. *J. Phys. Lett.* **44** (1), 1–12.

COLONIUS, T., LELE, S. K. & MOIN, P. 1997 Sound generation in a mixing layer. *J. Fluid Mech.* **330**, 375–409.

DOCQUIER, N. & CANDEL, S. 2002 Combustion control and sensors: a review. *Prog. Energy Combust. Sci.* **28** (2), 107–150.

DOWLING, A. P. 1992 Thermoacoustic sources and instabilities. In *Modern Methods in Analytical Acoustics*, chap. 13, pp. 378–403. Springer.

DOWLING, A. P. & FFOWCS WILLIAMS, J. E. 1983 *Sound and Sources of Sound*. Horwood.

DOWLING, A. P. & MAHMOUDI, Y. 2015 Combustion noise. *Proc. Combust. Inst.* **35**, 65–100.

DUNSTAN, T. D., SWAMINATHAN, N., BRAY, K. N. C. & KINGSBURY, N. G. 2013 Flame interactions in turbulent premixed twin V-flames. *Combust. Sci. Technol.* **185** (1), 134–159.

ECHEKKI, T. & CHEN, J. H. 1999 Analysis of the contribution of curvature to premixed flame propagation. *Combust. Flame* **118** (1), 308–311.

ECHEKKI, T., CHEN, J. H. & GRAN, I. 1996 The mechanism of mutual annihilation of stoichiometric premixed methane–air flames. *Symp. Intl Combust.* **26** (1), 855–863.

FLEMMING, F., SADIKI, A. & JANICKA, J. 2007 Investigation of combustion noise using a LES/CAA hybrid approach. *Proc. Combust. Inst.* **31**, 3189–3196.

FOGLA, N., CRETA, F. & MATALON, M. 2017 The turbulent flame speed for low-to-moderate turbulence intensities: hydrodynamic theory vs. experiments. *Combust. Flame* **175**, 155–169.

GRIFFITHS, R. A. C., CHEN, J. H., KOLLA, H., CANT, R. S. & KOLLMANN, W. 2015 Three-dimensional topology of turbulent premixed flame interaction. *Proc. Combust. Inst.* **35** (2), 1341–1348.

HAWORTH, D. C. & POINSOT, T. J. 1992 Numerical simulations of lewis number effects in turbulent premixed flames. *J. Fluid Mech.* **244**, 405–436.

HURLE, I. R., PRICE, R. B., SUGDEN, T. M. & THOMAS, A. 1968 Sound emission from open turbulent premixed flames. *Proc. R. Soc. Lond.* A **303** (1475), 409–427.

IHME, M. 2017 Combustion and engine-core noise. *Annu. Rev. Fluid Mech.* **49**, 277–310.

IHME, M. & PITSCH, H. 2012 On the generation of direct combustion noise in turbulent non-premixed flames. *Intl J. Aeroacoust.* **11** (1), 25–78.

IHME, M., PITSCH, H. & BODONY, D. 2009 Radiation of noise in turbulent non-premixed flames. *Proc. Combust. Inst.* **32** (1), 1545–1553.

JIMÉNEZ, C., HAGHIRI, A., TALEI, M., BREAR, M. J. & HAWKES, E. R. 2015 Sound generation by premixed flame annihilation with full and simple chemistry. *Proc. Combust. Inst.* **35**, 3317–3325.

KARAMI, S., HAWKES, E. R., TALEI, M. & CHEN, J. H. 2015 Mechanisms of flame stabilisation at low lifted height in a turbulent lifted slot-jet flame. *J. Fluid Mech.* **777**, 633–689.

KARAMI, S., HAWKES, E. R., TALEI, M. & CHEN, J. H. 2016 Edge flame structure in a turbulent lifted flame: a direct numerical simulation study. *Combust. Flame* **169**, 110–128.

https://doi.org/10.1017/jfm.2018.115 Published online by Cambridge University Press

KARAMI, S., TALEI, M., HAWKES, E. R. & CHEN, J. H. 2017 Local extinction and reignition mechanism in a turbulent lifted flame: a direct numerical simulation study. *Proc. Combust. Inst.* **36** (2), 1685–1692.

KEE, R. J., GRCAR, J. F., SMOOKE, M. D., MILLER, J. A. & MEEKS, E. 1985 Premix: a fortran program for modeling steady laminar one-dimensional premixed flames. *Sandia National Laboratories Report*.

KENNEDY, C. A., CARPENTER, M. H. & LEWIS, R. M. 2000 Low-storage, explicit Runge–Kutta schemes for the compressible Navier–Stokes equations. *Appl. Numer. Maths* **35** (3), 177–219.

KIDIN, N., LIBROVICH, V., MACQUISTEN, M., ROBERTS, J. & VUILLERMOZ, M. 1988 Possible acoustic source in turbulent combustion. *Dyn. Reactive Syst. Part 1: Flames* **1**, 336–348.

KOTAKE, S. & TAKAMOTO, K. 1990 Combustion noise: effects of the velocity turbulence of unburned mixture. *J. Sound Vib.* **139** (1), 9–20.

LAW, C. K. & SUNG, C. J. 2000 Structure, aerodynamics, and geometry of premixed flamelets. *Prog. Energy Combust. Sci.* **26** (4), 459–505.

LIEUWEN, T. C. 2012 *Unsteady Combustor Physics*. Cambridge University Press.

LIGHTHILL, M. J. 1952 On sound generated aerodynamically: I. General theory. *Proc. R. Soc. Lond.* A **211**, 564–587.

LIGHTHILL, M. J. 1954 On sound generated aerodynamically: II. Turbulence as a source of sound. *Proc. R. Soc. Lond.* A **222** (1148), 1–32.

LIU, Y. 2015 Two-time correlation of heat release rate and spectrum of combustion noise from turbulent premixed flames. *J. Sound Vib.* **353**, 119–134.

LIVEBARDON, T., MOREAU, S., POINSOT, T. & BOUTY, E. 2015 Numerical investigation of combustion noise generation in a full annular combustion chamber. *AIAA Paper* 2015-2971.

LOCKARD, D. P. 2000 An efficient, two-dimensional implementation of the Ffowcs Williams and Hawkings equation. *J. Sound Vib.* **229** (4), 897–911.

MIYAUCHI, T., TANAHASHI, M. & LI, Y. 2001 Sound generation in chemically reacting mixing layers. In *Smart Control of Turbulent Combustion*, pp. 28–38. Springer.

PASSOT, T. & POUQUET, A. 1987 Numerical simulation of compressible homogeneous flows in the turbulent regime. *J. Fluid Mech.* **181**, 441–466.

POINSOT, T., ECHEKKI, T. & MUNGAL, M. G. 1992 A study of the laminar flame tip and implications for premixed turbulent combustion. *Combust. Sci. Technol.* **81** (1–3), 45–73.

POINSOT, T. & VEYNANTE, D. 2005 *Theoretical and Numerical Combustion*. RT Edwards, Inc.

RAJARAM, R., GRAY, J. & LIEUWEN, T. 2006 Premixed combustion noise scaling: total power and spectra. *AIAA Paper* 2006–2612.

RAJARAM, R. & LIEUWEN, T. 2009 Acoustic radiation from turbulent premixed flames. *J. Fluid Mech.* **637**, 357–385.

SCHULLER, T., DUROX, D. & CANDEL, S. 2003 Self-induced combustion oscillations of laminar premixed flames stabilized on annular burners. *Combust. Flame* **135** (4), 525–537.

SILVA, C. F., LEYKO, M., NICOUD, F. & MOREAU, S. 2013 Assessment of combustion noise in a premixed swirled combustor via large-eddy simulation. *Comput. Fluids* **78**, 1–9.

SMITH, G. P., GOLDEN, D. M., FRENKLACH, M., MORIARTY, N. W., EITENEER, B., GOLDENBERG, M., BOWMAN, C. T., HANSON, R. K., SONG, S., GARDINER, W. C. L. JR *et al.* 1999 GRI 3.0 Mechanism. *Gas Research Institute* (http://www.me.berkeley.edu/gri_mech).

SMITH, T. J. B. & KILHAM, J. K. 1963 Noise generation by open turbulent flames. *J. Acoust. Soc. Am.* **35**, 715–724.

STRAHLE, W. C. 1978 Combustion noise. *Prog. Energy Combust. Sci.* **4** (3), 157–176.

STRAHLE, W. C. & SHIVASHANKARA, B. N. 1975 A rational correlation of combustion noise results from open turbulent premixed flames. *Symp. Intl Combust.* **15** (1), 1379–1385.

SUN, C. J. & LAW, C. K. 1998 On the consumption of fuel pockets via inwardly propagating flames. *Symp. Intl Combust.* **27** (1), 963–970.

SWAMINATHAN, N., BALACHANDRAN, R., XU, G. & DOWLING, A. P. 2011*a* On the correlation of heat release rate in turbulent premixed flames. *Proc. Combust. Inst.* **33** (1), 1533–1541.

https://doi.org/10.1017/jfm.2018.115 Published online by Cambridge University Press

SWAMINATHAN, N., XU, G., DOWLING, A. P. & BALACHANDRAN, R. 2011*b* Heat release rate correlation and combustion noise in premixed flames. *J. Fluid Mech.* **681**, 80–115.

TALEI, M., BREAR, M. J. & HAWKES, E. R. 2011 Sound generation by laminar premixed flame annihilation. *J. Fluid Mech.* **679**, 194–218.

TALEI, M., BREAR, M. J. & HAWKES, E. R. 2012*a* A parametric study of sound generation by premixed laminar flame annihilation. *Combust. Flame* **159** (2), 757–769.

TALEI, M., BREAR, M. J. & HAWKES, E. R. 2014 A comparative study of sound generation by laminar, combusting and non-combusting jet flows. *Theor. Comput. Fluid Dyn.* **28** (4), 385–408.

TALEI, M., HAWKES, E. R. & BREAR, M. J. 2012*b* A direct numerical simulation study of frequency and Lewis number effects on sound generation by two-dimensional forced laminar premixed flames. *Proc. Combust. Inst.* **34**, 1093–1100.

TANAHASHI, M., TSUKINARI, S., SAITOH, T., MIYAUCHI, T., CHOI, G.-M., IKAME, M., KISHI, T., HARUMI, K. & HIRAOKA, K. 2002 On the sound generation and its controls in turbulent combustion field. In *Proceedings of 3rd Symposium on Smart Control of Turbulence*, pp. 149–160. University of Tokyo, Japan.

WU, X. & MOIN, P. 2008 A direct numerical simulation study on the mean velocity characteristics in turbulent pipe flow. *J. Fluid Mech.* **608**, 81–112.

YOO, C. S. & IM, H. G. 2007 Characteristic boundary conditions for simulations of compressible reacting flows with multi-dimensional, viscous and reaction effects. *Combust. Theor. Model.* **11** (2), 259–286.

ZHANG, F., HABISREUTHER, P., BOCKHORN, H., NAWROTH, H. & PASCHEREIT, C. 2013 On prediction of combustion generated noise with the turbulent heat release rate. *Acta Acust.* **99** (6), 940–951.

ZHAO, W. & FRANKEL, S. H. 2001 Numerical simulations of sound radiated from an axisymmetric premixed reacting jet. *Phys. Fluids* **13** (9), 2671–2681.

https://doi.org/10.1017/jfm.2018.115 Published online by Cambridge University Press